Chapter 1

1.1 Introduction

Nanomaterials, which have very tiny dimensions of 100 nm or less, are the foundations of nanotechnology in general. The physical and chemical characteristics of nanoparticles differ from those of bulk materials, and they might behave differently as a result. Their physical, optical, magnetic, electrical, mechanical, and transport features arise at this nanoscale [1]. Nanomaterials have two distinguishing characteristics: increased surface area and quantum behaviour. The fraction of atoms on the surface of materials grows proportionately as the quantity of surface area per unit volume ratio increases from bulk to nano form, which accounts for the amazing features of nanomaterials [2]. Because chemical reactions take place largely on surfaces, the reactivity of a given quantity of materials in nanoform is higher than in bulk form. The use of the volume-specific surface area (VSSA) as a simple criterion to identify nanoparticles is advocated by the EU definition of nanomaterials [3]. Quantum confinement in nanostructures like quantum wells and quantum dots also provides exceptional optoelectronic features [4,5].

1.2 Dimensional categorization of nanomaterials

The number of dimensions that aren't restricted to the nanoscale range (less than 100nm):

(a) Zero-dimensional (0-D): All dimensions (x,y,z) at nanoscale. For example, nanoparticles.

(b) One-dimensional (1-D): At the nanoscale, there are just two dimensions (x,y) and no additional dimension. For example, nanorods, nanotubes, and nanowires.

(c) Two-dimensional (2-D): At the nanoscale, just one dimension exists. The other two dimensions, however, are not. For example, nanofilms, nanocoatings, etc.

(d) Three-dimensional (3-D): Bulk materials that aren't restricted to the nanoscale. Materials have a nanocrystalline structure or nanoscale characteristics. For example, nanoparticle dispersions, nanowire bundles, nanotubes, and multinanolayers.

Fig.1.1 shows different allotropes of carbon with different dimensions.

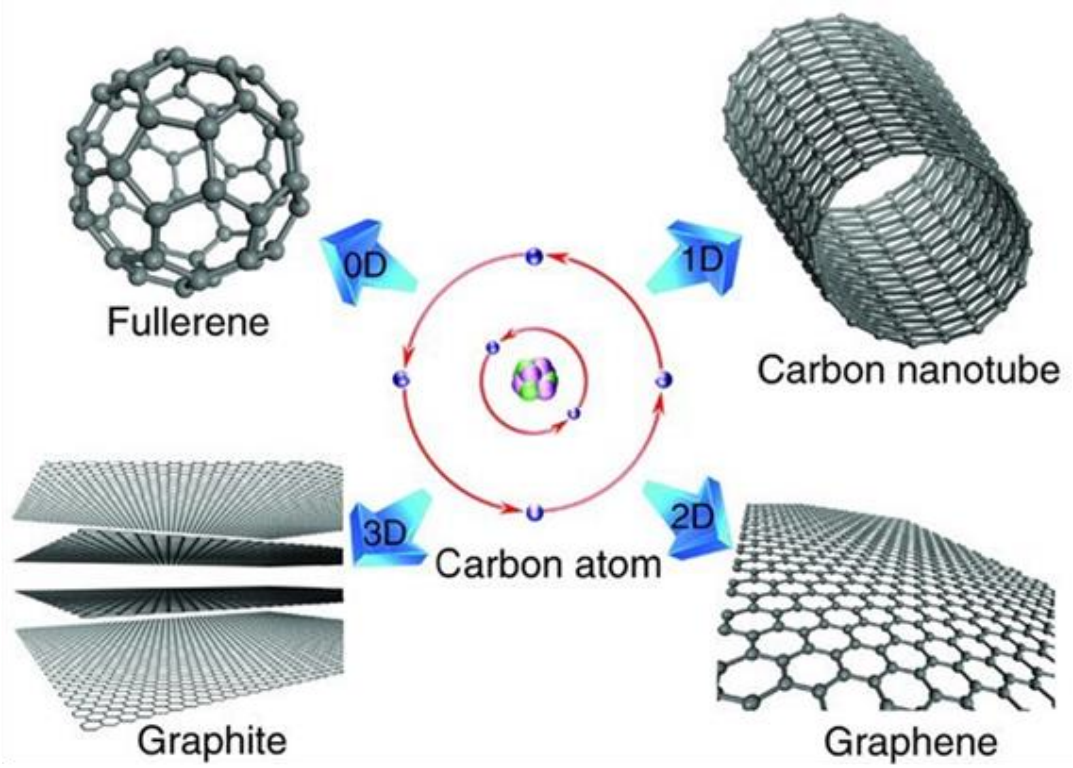

Fig. 1.1 Carbon allotropes with different dimensions [6].

1.3 Brief history of Carbon and Carbon Nanomaterials

In 1772, Antony Lavoisier discovered Carbon. Its atomic number is 6 and the symbol is C. It is non-metallic and has valency 4. There are various allotropes of carbon but mainly three are naturally occurring i.e. graphite, amorphous carbon and diamond. Carbon atoms may be bonded in several ways, resulting in various carbon allotropes. Graphite, diamond, and Buckminster fullerenes are examples. Diamonds are exceedingly clear, but graphite is opaque and black, indicating that various allotropes of carbon have varied physical qualities. Diamond is the hardest natural substance, but graphite is quite soft. Diamond possesses low electrical conductivity while graphite is having high electrical conductivity. When it comes to abrasives, diamond is the clear winner, but graphite is a close second. The thermal conductivity of diamond is good than that of graphite. Another allotrope of carbon is the amorphous carbon comprised of sp^2 and sp^3 hybridised carbon in varying ratios, missing in crystallinity. It is the primary constituent of activated carbon, charcoal, and lamp black. Several other allotropes of

carbon have now been synthesized like fullerenes which include carbon nanotube [7], buckyball [8], carbon nanobud [9] and carbon nanofibers [10]. Linear acetylenic carbon [11,12], carbon nanofoam [13], lonsdaleite [14] also come in the category of carbon allotropes.

1.3.1 Graphite

"Graphite" is a mineral and an allotropic form of carbon with a crystal structure. It is the most prevalent and thermodynamically viable allotrope of carbon at low pressure, whereas the converse is true at high pressure. At 25 °C, the typical free energy for converting graphite to diamond is 2.90 $kJmol^{-1}$. It is made up of parallel layers of sp^2 hybridised carbon atoms (graphene sheets) with fused hexagonal rings held together by weak van der walls forces. In graphite, the layers are layered in an AB pattern. This resulted in a hexagonal unit cell having dimensions c = 6.71 Å and a = 2.46 Å. Only four atoms are present in the unit cell labelled as A, A′, B, B′ in Fig.1.2. A and B atoms are present on one layer and A′, B′ atoms are present on a different layer which is a distance of half of the crystallographic *c*-axis spacing i.e., 3.35 Å. The A and A′ atoms have atoms above and below directly in the adjacent layer while B and B′ atoms do not. The atoms B and B′, have neighbours directly above and below in layer planes which are at a distance of 6.71 Å. Its crystal structure matches the space group $P6_3/mmc$. Its structure has an inversion symmetry centre at the AA′ distance midway [15]. Graphite is anisotropic due to the different bonding in in-plane and out-of-plane. Because graphite's elastic modulus is aligned in the plane rather than out of a plane, it is harder in the plane than diamond. Because of its layered structure, which allows layers to travel past one other, it has lubricating qualities. This allotrope is also electrically conductive, making it a useful electrode material. This ability stems from the delocalization of π-electrons in fused hexagonal carbon rings in plain, but with lower electrical conductivity in-plane vertical to the graphitic plane. This results in a decrease in the bulk electrical conductivity.

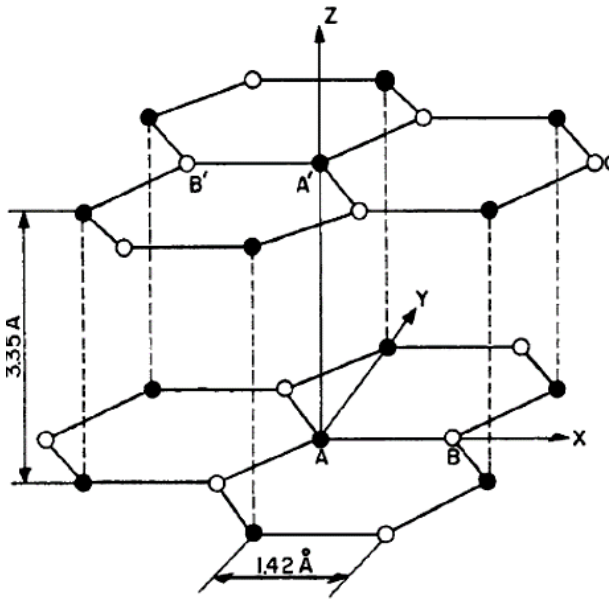

Fig. 1.2 Graphite's crystal structure [16].

1.3.2 Diamond

Diamond's cubic three-dimensional lattice is a meta-stable form of carbon with a carbon-carbon bond length of 1.54Å and a lattice constant of 3.57. Each carbon atom is sp^3 hybridised and tetrahedrally linked to four others [17]. Its less common hexagonal form is interconvertible at some standard conditions [18]. It is also the hardest material which is used as an abrasive material that can stand abrasion in the course of friction. Its high thermal conductivity (up to 2,200 W/(m·K)) properties make it useful in heat sinks application. This is because of the low phonon scattering present between the carbon atoms of the diamond. In addition to having a 5.5 eV wide band gap, high electric field breakdown, a low dielectric constant, a durable nature, and biocompatibility, diamond also has several other properties [19-23].

1.3.3 Carbon in the nano-crystalline forms

At the close of the 20th century, the nano-crystalline forms of carbon, such as fullerene, carbon nanotubes, carbon fibres, graphene, nanodiamond, and carbon nanoscrolls, were discovered thanks to advances in science and technology.

1.3.2.1 Fullerene

In 1985, Harold et al. identified a novel carbon allotrope in which the atoms are organised in closed shells [24]. American architect Richard Buckminster Fuller, whose 1960s geodesic domes resemble the structure of spherical fullerenes, was the origin of the name fullerene. It is a zero-dimensional form of carbon-caged molecules having polyhedral structures. Instead of having graphite-like structures, it also contains pentagons and sometimes heptagons of carbon atoms in its structure. The Buckminsterfullerene (C60) molecule, which consists of 60 carbon atoms, is the member of this family that is the most stable. It is the foundation for the construction of a closed cage with icosahedral symmetry and consists of twenty hexagonal rings and twelve pentagonal rings. All carbon atoms are sp^2 hybridised, which implies they are all joined by three additional carbon atoms. The C60 molecule is made up of six: six ring bonds, which are referred to as "double bonds" and are shorter than six: five ring bonds. Fullerene has an average bond length of 0.14 nm. According to the icosahedra-making laws, an infinite number of fullerenes can exist. When the number of pentagons remains constant but the number of hexagons varies, a variety of fullerenes of various sizes and shapes results (C72, C80, etc.). Buckminsterfullerene has excellent semiconducting [25], magnetic [26], and superconducting characteristics [27].

1.3.2.2 Carbon nanotube

Iijima (1991) found multi-walled carbon nanotubes(MWCNT) in arc-discharge carbon soot following the discovery of bulk synthesis of fullerenes [28]. Two years later, he disclosed the production of single-walled nanotubes [29]. Carbon nanotubes are tubular carbon compounds produced from sp^2 hybridised graphene sheets that have been wrapped around one another. The most prevalent varieties are single-walled carbon nanotubes (SWCNT) and multi-walled carbon nanotubes (MWCNT). SWCNT is made out of a single graphene sheet that has been smoothly wrapped around a cylindrical tube. MWCNT, on the other hand, is made up of concentric tubes of graphene sheets. The chiral vector (C_h) also known as the rolled-up vector, and the chiral angle (θ)determine the structural information of nanotubes [30]. The amount of 'twist' in the tube is determined by the chiral angle. The chiral angle determines the zig-zag and armchair shape of carbon bonds around the perimeter of the nanotube.

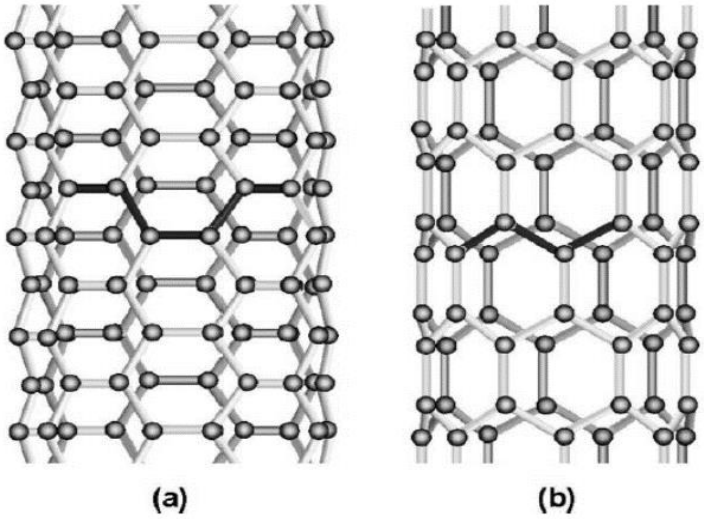

Fig. 1.3 Schematic diagram showing how a hexagonal sheet of graphite is 'rolled' to form a carbon nanotube [30].

If you roll the graphite sheet in the a_1 direction, you'll get a zig-zag nanotube. Armchair nanotubes were created by rolling graphite sheets in the chiral vector (C_h) direction.

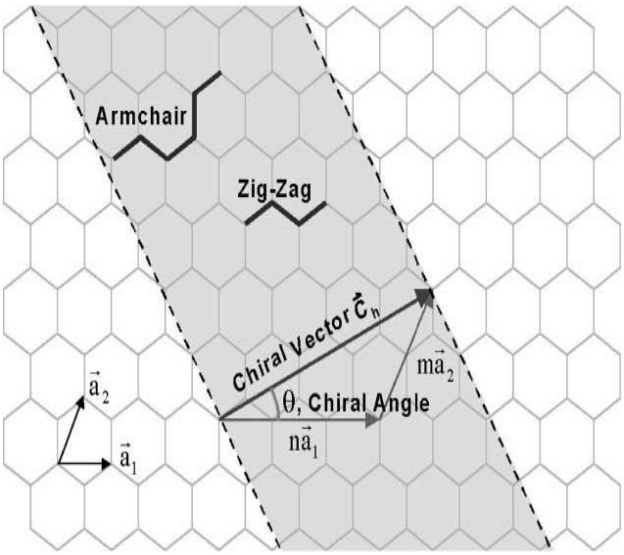

Fig. 1.4 Depiction of the atomic structure of (a) an armchair and (b) a zig-zag nanotube [30].

Carbon nanotube chirality affects their electrical properties. Graphite is a semi-metal, but nanotube chirality determines whether they are metallic or semiconducting [31]. Multiwall carbon nanotubes have 0.34 nm wall spacing, equivalent to graphite. Multiwalled nanotube structures were described using the Russian doll and Swiss roll models. In the Swiss roll or Parchment form, a single layer of graphite is rolled over itself, whereas the Russian doll type features concentric cylinders [32,33].

1.3.2.3 Graphene

With a carbon-carbon bond length of 0.142 nm, graphene is a single-layer, two-dimensional (2D) honeycomb structure comprised of carbon atoms [34]. The quantum hall effect and lack of delocalization are caused by the behaviour of graphene electrons as massless relativistic particles[35,36]. It demonstrates many intriguing characteristics, such as significant thermal conductivity ($5000 Wm^{-1} K^{-1}$) [37], high electron mobility at ambient temperature (250,000 cm^2/Vs) [38], and exceptional mechanical properties with Young's modulus of 1 TPa [39]. The word graphene was coined by Hans-Peter Boehm in 1962 to describe each carbon layer in graphite intercalated compounds [40]. Graphite has been used to adorn ceramics for over 6000 years, but research on graphene (a single sheet of graphite) began in 1960 when the strong conductivity of graphitic basal planes in graphite intercalated compounds was discovered [41-43]. As a result, scientists were ecstatic about the discovery, which might lead to a low-cost alternative to metal conductors. Then, near the close of the twentieth century, research began with the goal of studying graphene layers for their exceptional electrical characteristics. In graphite intercalated compounds, large molecules were sandwiched between adjacent planes, creating isolated graphene layers in a three-dimensional matrix. As more molecules are removed, stacked and scrolling structures with no structural control are produced. Two-dimensional materials are thought to be unstable and unable to exist without a three-dimensional base. A graphene sheet is thermodynamically unstable below 20 nm, according to ab initio simulations. With up to 6000 carbon atoms, graphene is the least stable, and with about 24,000 carbon atoms, it is the most stable (as in graphite). For single-layer graphene, the unit cell is made up of two types of carbon atoms, A and B, that form a triangular 2-D network but are separated by the C-C distance a_{c-c} =1.42 nm [44,45].

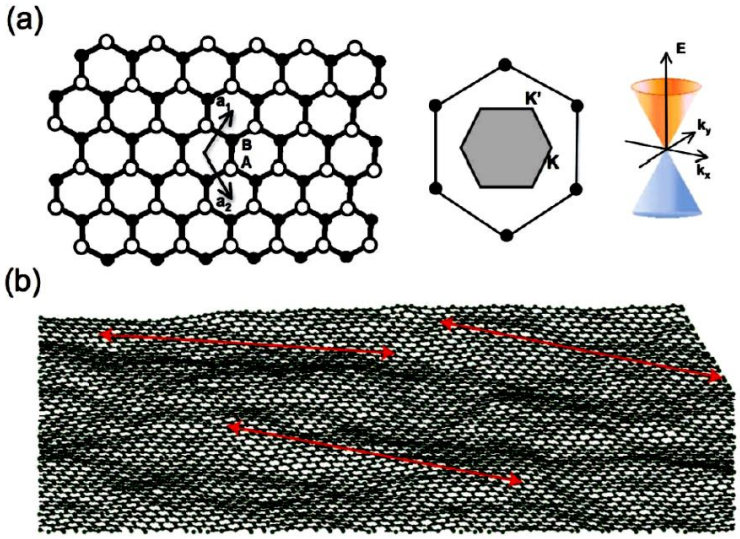

Fig.1.5 (a) Illustrations of the graphene crystal structure, Brillouin zone, electronic dispersion spectrum, and (b) "Rippled graphene" simulation using a Monte Carlo method. The length of the red arrows is around 8 nm [46].

1.3.2.4 Carbon nanofiber

Hughes and Chambers' patent on the manufacture of filamentous carbon, issued in 1889, is one of the first technical reports on carbon nanofibers. They generated carbon filaments by carbon deposition using a methane/hydrogen gaseous mixture in a gas pyrolysis method [47,48]. Cylindrical nanostructures are present in CNFs, and these nanostructures may stack graphene sheets in a variety of forms, such as stacked platelet, ribbon, or herringbone [49]. Their diameter can range anywhere from a few 10's nanometers and a few 100's nanometers and their length is approximated in micrometres. CNFs have mechanical and electrical characteristics that are comparable to CNTs. Although their size and graphitic arrangement can be controlled [50,51]. As a result, as compared to CNTs, CNFs have a larger surface area with more functional groups. As a result, biomolecules can be immobilised on the surface of CNFs. CNFs, on the other hand, vary from traditional carbon fibres and vapour-grown carbon fibres (VGCFs) because of their tiny diameter. The diameters of conventional carbon fibres and VGCFs are several micrometres [52].

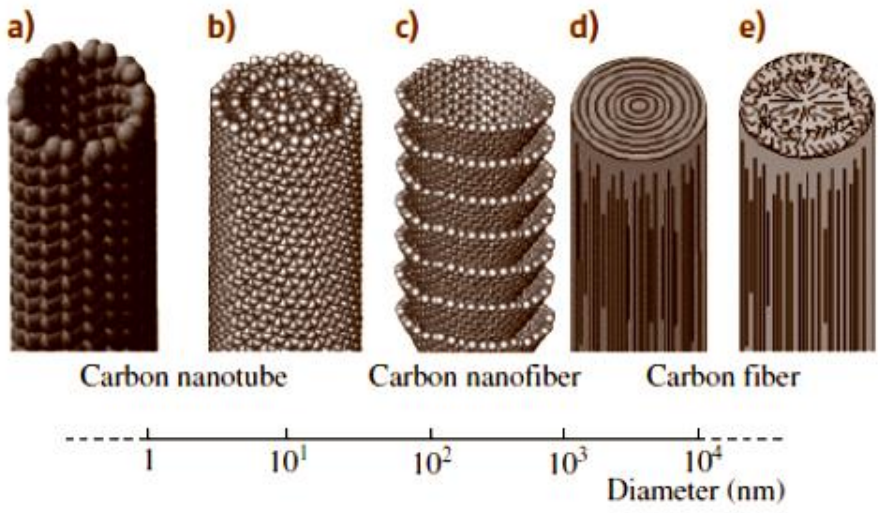

Fig.1.6 Log scale diameter comparison of fibrous carbon compounds [53].

1.3.2.5 Carbon nanoscroll

Carbon nanoscrolls (CNS) were made up of folded graphene sheets with open ends and graphite-like interlayer spacing. Bacon described the synthesis of CNS as scrolling whiskers in 1960 [54,55]. The volume of the carbon nanoscrolls is approximately six times that of the graphite precursor material. The oxidation of nanoscrolls occurs around 450°C, which is lower than that of graphite starting material (which is stable in the air up to 650°C). This is because there are fewer van der Waals contacts than there were in the initial graphite powder. The tests indicate that carbon nanoscrolls may have a sizable surface area. In theory, carbon sheets are capable of having a surface area of up to 2630 m^2/g [56], provided that both sides of the sheet are accessible. This is achievable with open-ended carbon nanoscrolls, but it is not conceivable with capped carbon nanotubes. The CNS is predicted to have qualities that are halfway between carbon nanotubes and graphene. CNS has strong electrical and thermal conductivity due to π-electrons along the sp^2 carbon sheet. The CNS may expand in volume thanks to the rolled sheet structure, which is advantageous in a variety of applications such as supercapacitors and batteries [57,58]. Because CNS can generate intercalation compounds with lithium ions, it can be employed as a cathode in lithium-ion batteries. CNS interlayer distance variation is beneficial for hydrogen storage.

1.3.2.6 Nanodiamond

The structure and characteristics of a nanodiamond (ND) are similar to those of a diamond. The average diameter is around 5nm. "Nanodiamond" refers to numerous types of diamond at the nanoscale (length scale of 1–100 nm). To produce nanodiamonds at the lab scale, many preparation techniques have been created. Nanodiamond is made using two main methods: graphite transformation at high temperatures and pressures, and detonation of carbon explosive materials. Bundy et al. described a high-pressure, high-temperature diamond production technique[59]. Diamond synthesis via explosive detonation, on the other hand, was first described in the 1980s[60]. Explosive detonation is still frequently utilised, however, the detonator explosion process is incredibly rapid and complicated. A synthetic diamond's quality depends heavily on its manufacturing process. Certain synthetic diamonds may exceed most naturally generated diamonds in terms of hardness, thermal conductivity, and electrical conductivity. Synthetic diamonds have been used in a variety of products, including abrasives, cutting and polishing tools, and heat sinks. Electrical components that use synthetic diamonds include high-power switches, field-effect transistors, and light-emitting diodes. In high-power CO_2 lasers and gyrotron, synthetic diamond is currently used for optical windows due to its chemical and thermal durability, low thermal expansion, and excellent optical transparency over a broad spectrum range. It is anticipated that 98% of the diamonds utilised in industrial applications will be synthetic diamonds.

1.4 Applications of Carbon Nanomaterials and Polymer Composites

1.4.1 Thin film filed effect transistor

1.4.1.1 Conductive polymers

Conductive polymers (CPs) represent an area of an organic semiconductor having peculiar electrical and optical properties. Due to its low-cost synthesis, material processability, lightweight, tunable electrical conducting property, and flexibility, replacing amorphous silicon in the electronic industry [61,62]. The conductive polymer and their composites provide a vast number of applications such as supercapacitors [63], light-emitting diodes [64], solar cells [65], field-effect transistors [66], sensors [67,68], Biosensors [69], batteries [70], corrosion inhibition [71], etc. These devices have

utilized conducting polymers like polypyrrole, polyaniline, polythiophene , etc. as active materials. Processability into a thin film on various substrates and the steps for choosing materials with good electrical conductivity are important from the perspective of organic polymer electronic devices. The economic factor also plays an important role but can be ignored for the superior quality range of products. Thus developing a reliable technique to incorporate organic material in low-cost device fabrication has attracted the attention of researchers. Another important parameter of material selection is its electronic structure. The molecular interactions present in the organic molecules make them resistant to modification in their assembly(ordering of π-conjugated polymer chain). The molecular interactions can be tuned by introducing templates or through self-assembly to improve the crystallinity of CPs [72,73]. By alignment of CPs, charge carrier mobility can be enhanced in large-area electronics applications [74,75].

1.4.1.2 Brief introduction of charge transport in π-conjugated CPs

The π-conjugated CPs have an exclusive electronic and optoelectronic properties like those of inorganic semiconductors and metals having conjugation in the carbon chain. Charge delocalization along the polymer chain is enabled by the π-electrons being delocalized inside the unsaturated carbon chain backbone [76,77]. The research on CPs has become more intense after the discovery of poly-sulphur nitride showing superconductivity at low temperatures in 1975 [78]. The significant change occurred when Shirakawa, Macdiarmid, and Heeger found electrical conductivity in trans polyacetylene in 1977. The electrical conductivity was enhanced by several orders from 10^{-9} Scm^{-1} to 10^{5} Scm^{-1} by doping with an oxidizing agent like I_2 [79]. Then, researchers concentrated on improving the conductivity of derivatives of polyacetylene[80]. Thus Shirakawa, Macdiarmid, and Heeger got the noble prize for this outstanding discovery in 2000 [81]. Typical CPs are poly para phenylene, polypyrrole, polythiophene, poly-indole, polyaniline, polycarbazole, polyfuran, etc. In terms of electronic device application, thiophene polymers have gained significance due to their environment stability, thermal stability, solution processability, and excellent charge carrier mobility. The delocalized π- electrons do not introduce conductivity to the polymers i.e. the pristine form is still insulating. The electrical and optical characteristics of thiophene polymers may be modified by doping or chemical modification; for example, their bandgap ranges from 3 to 1 eV relying on the doping

concentration and side-chain groups attached [82]. Doping is a redox process that results in a p or n-type conjugated system. Chemical, electrochemical, photodoping, and charge injection doping are all options for doping [81]. When polymer unit cells connect and create electrical bands, it behaves similarly to crystals. The inherent electronic characteristics of these polymers are controlled by the bandgap(E_g) between HOMO and LUMO. As seen in Fig. 1.7, the vertical ionisation procedure in polymers creates a hole in the valence band [83]. There are three crucial factors to take into account: (i)the positive charge is free to move over the whole chain, (ii)there is no lattice distortion on the chain, and (iii) the existence of a hole or unfilled level at the valence band gives the material a metallic appearance. According to the first assumption regarding charge transfer in the doped organic polymer, this is correct. A local distortion (relaxation) occurs around the charge in organic polymer chains, which introduces electronic states into the gap and forms a polaron, as seen in Fig. 1.7.

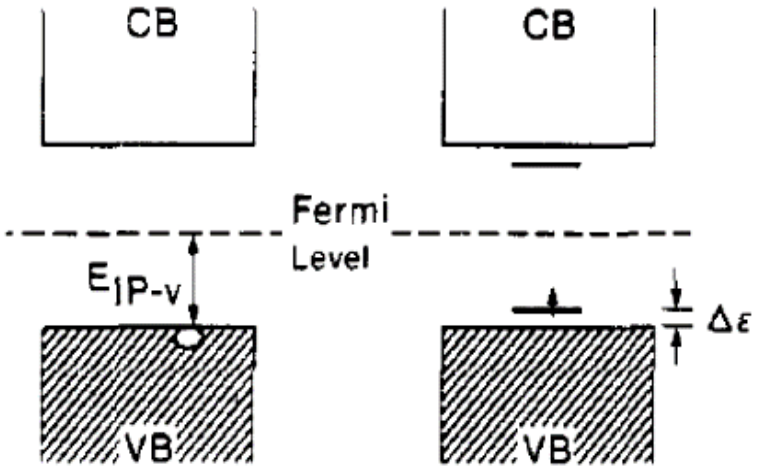

Fig.1.7 A polymeric chain's band structure is depicted in the case of (a) ionisation and (b) the production of a polaron. The Fermi level or chemical potential is used as a reference level [83].

The localised electronic states are known as polaronic states and the polaron is only a radical ion with spin (1/2), and charge (1e), coupled with lattice distortion. In the case of polaron generation, the valence band remains filled while the conduction band is still empty. The removal of a second electron from the polymer chain results in the formation of bipolarons. It is referred to be a pair of comparable charges with local lattice distortion. In the event of p or n-type doping, bipolaron levels existing in the gap are either empty or filled, rendering them spinless. Two optical transitions from the VB to the lower bipolaron level and the VB to the higher bipolaron level are theoretically possible below the bandgap transition. Both of these transitions take place below the bandgap transition (Fig. 1.8 a). There could be a third absorption in the case of polarons below the gap, which would be analogous to an optical transition between the two polaron levels (Fig. 1.8a).

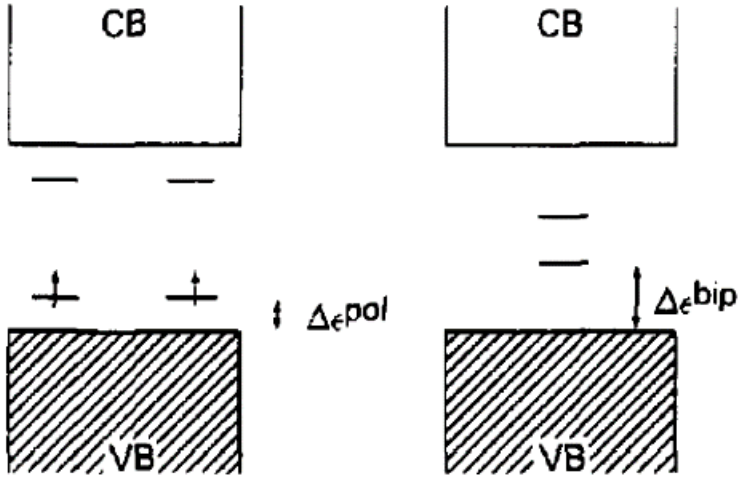

Fig.1.8 A polymer chain's band structure: (a) two polarons; (b) one bipolaron [83].

Two geometric configurations have the same energy in trans- polyacetylene's degenerate ground state. The experimentally altered bond length by Δr is 0.08Å. The bipolaron created can readily dissociate due to the degeneracy. As a result, the geometric structures that exist between the two charges are comparable to those that exist outside of the charges. As a result, there is no increment in deformation energy while changing from one geometric shape to another. Chain segments are separated by a barrier brought about by the isolated charge on t-polyacetylene. The two distinct structures in fig. 1.9 correspond to two potential wells. Solitons are the charges associated with the boundary wall. A neutral soliton, a radical that is equivalent to a soliton, is created when an odd number of carbon atoms in a chain have one unpaired electron apiece. In the midgap, electronic localised levels can be observed. They are empty or twice occupied when a soliton is positively charged or negatively charged, or half occupied when a soliton is neutral**.**

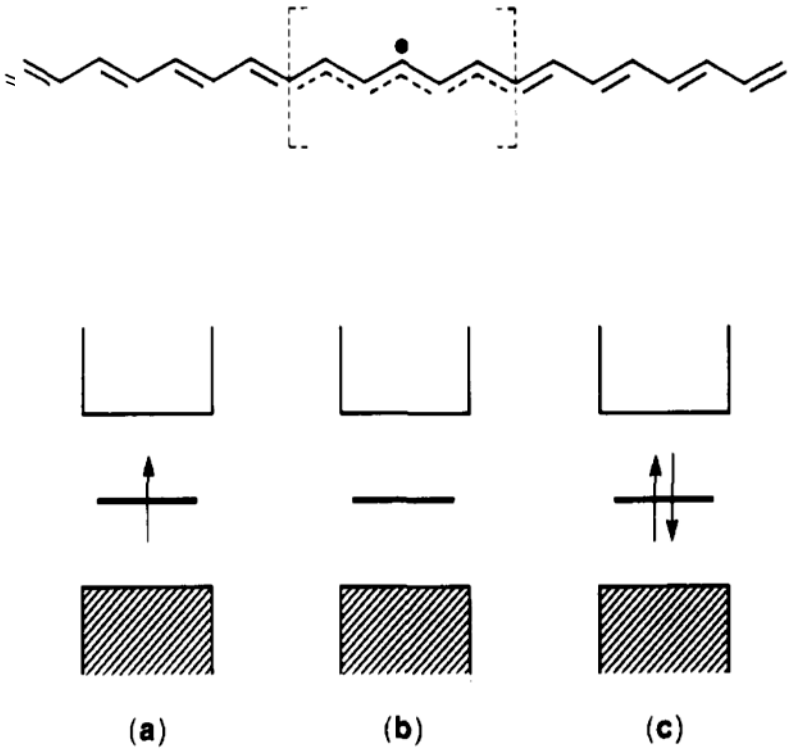

Fig. 1.9 Top: Schematic representation of a neutral soliton's geometric structure on a trans-polyacetylene chain. Band structure for a trans-polyacetylene chain with (a) neutral, (b) positively charged, and (c) negatively charged solitons are shown at the bottom [83].

The non-degenerate ground states of poly para phenylene, polypyrrole, and polythiophene all belong to the same geometric arrangement. A quinoid-like arrangement might contain more energy. The aromatic structure has lower ionisation energy and a better attraction for electrons than the quinoid structure, according to ab-initio calculations. Chain geometry in such compounds relaxes around this charge because the quinoid structure has a stronger affinity for electrons [84].

1.4.1.3 Polythiophene polymer

The polythiophene polymer is first synthesized in the year 1980 [85]. Due to its highly conducting and environmentally stable in comparison to other polymers, the various derivatives of polythiophene have been utilised in many electronic device-based

applications [86,87]. The insolubility of polythiophene polymers in various organic solvents is because of backbone rigidity, intramolecular interaction and crystallinity that suppress uniform doping, and solution processability on substrates. For the formation of efficient device fabrication, the uniaxial crystallisation of polymer is very important [88,89]. The solubility of thiophene may be further enhanced by adding an alkyl side chain to the third position, a process known as poly (3-alkylthienylenes). [90].Then further work has been done on poly (3- alkylthienylenes)thin film having good crystallinity and orientation [91,92]. Polythiophenes that contain head(H) to head(H) (2, 2' coupling) or tail(T) to tail(T) (5, 5' coupling) couplings are termed as regioirregular .while those which contain head to tail couplings (2,5' coupling) are called regioregular. Regioirregular polymers are not able to attain planar conformations while regioregular poly (3- alkyl thiophene) underwent self-assembly in both solid and solution phases to form highly ordered polymer structures possessing good electronic and optoelectronic properties. The attached linear side chain has strong interdigitation that is dependent on the side chain's location and length, and it has good solubility. Thin-film transistors made with regioregular poly (3-alkyl thiophene) have better charge transfer than those made of regio-random polythiophene.

1.4.1.4 Orientations of polymer chains and Intrachain and interchain charge transport

The thiophene polymer chain on the solid substrate can be positioned in one of three ways: (i) polythiophene crystallites with π-π stacking perpendicular to the substrate are called face-on oriented, (ii) those with π-π stacking parallel to the substrate are called edge-on oriented. These orientations are common in regioregular polymers (3- alkyl thiophene). There is another position known as flat-on, which is relatively uncommon. The polythiophene polymer chain is perpendicular to the substrate in this example [93,94].

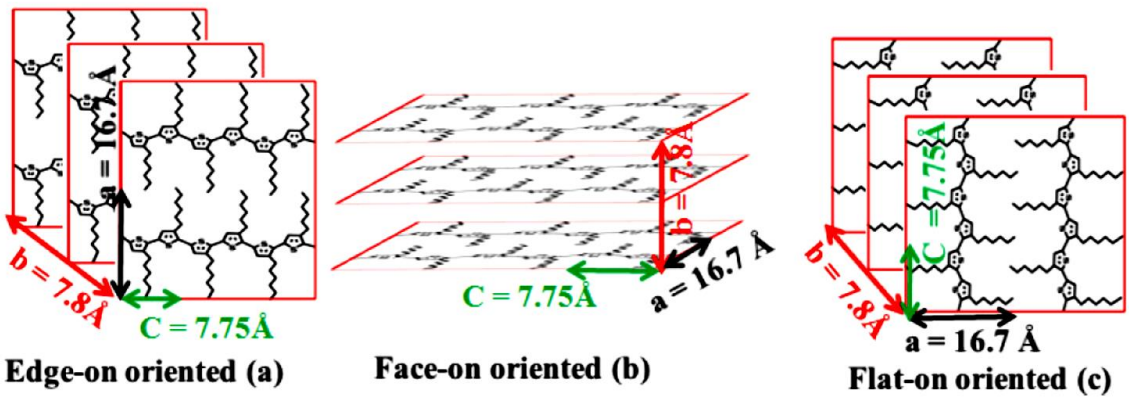

Fig. 1.10 "Edge on" (a) "face on" (b) and, "Flat-on" (c) orientation of regioregular PTs [94].

In regioregular poly (3-alkyl thiophene), charge transport is anisotropic. Charge transfer is discovered to take place along the polymer backbone, in both the conjugation and π-π stacking orientations (hopping). Only ordered structures were used for hopping transit. OFET is manufactured with crystallites oriented edge-on and face-on as seen in Fig.1.11. In edge-on crystallites, charge transfer occurs via π-π conjugation along the polymer chain as well as hopping, or interchain transport. Hoping through π-π stacking is restricted due to the insulating nature of the alkyl chain. Polythiophene polymers of various molecular weights are investigated for their ability to carry charge carriers in well-ordered polymer crystallites up to their contour length. The mobility of charge carriers is increased by utilising a polymer with a long conjugation because the long chain connects the crystalline domain, reducing the grain border and disordered area [95,96].

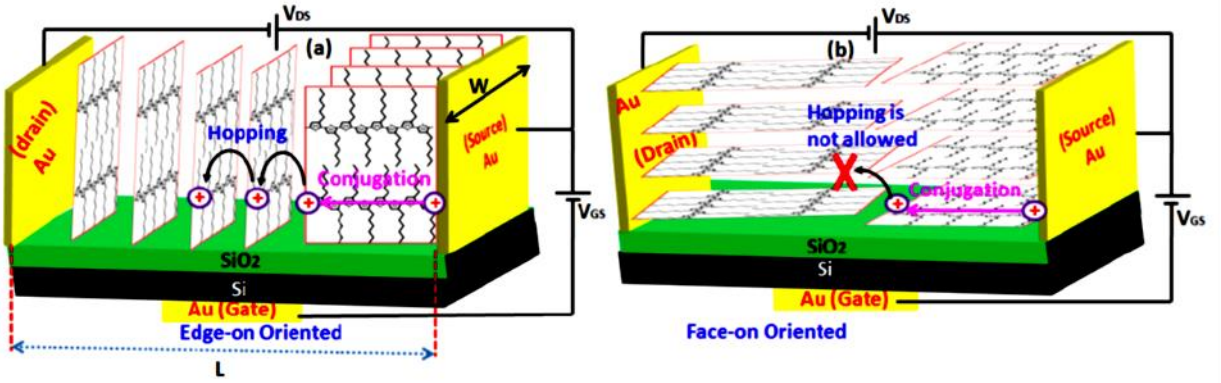

Fig. 1.11 Charge transport in OFET is fabricated using (a) edge-on oriented and (b) face-on oriented polymer chains [94].

1.4.1.5 Poly(2,5-bis(3-alkylthiophen-2-yl)thieno[3,2 b]thiophene)(PBTTT)

When it comes to creating alkyl thiophene-type polymers, there are three major drawbacks: (i)non-centrosymmetric essence of monomer, limiting the use of multiple techniques that aid in the synthesis of regular repeat units to obtain highly crystalline thin films [97,98], (ii)oxidative destabilisation due to highly delocalised e-rich π-system [99], (iii) Interdigitation and ordering are hampered by excessive side chain richness, which lowers intermolecular organisation at a long distance [100]. Thienothiophene copolymers are meant to overcome the thiophene polymer's molecular structural restrictions. Thieno[3,2-b]thiophene and 4,4-dialkyl 2,2-bithiophene monomer units periodically form the copolymer known as Poly(2,5-bis(3-alkyl thiophen-2-yl)thieno[3,2 b]thiophene) (PBTTT). The thieno[3,2-b]thiophene monomer helps in conjugation in neighbouring thiophene units attached at the 2^{nd}, and 5^{th} positions, because sulphur atoms are present in the anti position in thieno[3,2-b]thiophene, enabling π-electron delocalisation and so having lower bandgap and ionisation potential in PBTTT. The alkyl groups present in bithiophene donate σ electrons to π-electron systems by inductive effect. Thus, the ionisation potential of the conjugated thiophene polymer backbone is raised by the reduction of multiple alkyl groups. The conjugation electron density in PBTTT is decreased by the thieno[3,2-b]thiophene unit when not substituted. The likelihood of electrons from the fused thienothiophene ring being delocalized to the backbone is thereby reduced. Therefore the quinoidal form of high

energy is less favourable to thienothiophenes and also reduction of electron density due to fewer alkyl chains gives the HOMO level of pBTTT lower than P3HT(poly-3 hexyl thiophene).In π-conjugated polymer, the coplanarity of aromatic units provides good coherent conjugation along the backbone that gives a small bandgap, rapid intramolecular charge transport, less reorganization energy and close intermolecular packing. Also, the strong π-π interactions between coplanar backbones promote self-assembly in solution and form an ordered structure in solid-state [101,102]. The PBTTT conjugated backbone units adopt a coplanar conformation and enable adjacent polymer backbones to settle close to each other with tilted conjugated plane units. This helps in an extended order feature called π-stacked lamella which is due to the planarity of monomers [103,104]. With π-stacking of the polymer chains, charge transfer takes place between and along the chain in two dimensions in addition to one dimension. As a result, the polymer backbone acts as a stiff rod-like structure, allowing for π-stacking and interdigitation of side chains between stacked lamella, resulting in more organised and sideways expanded microstructures.

The microstructure and thermal properties of thin films are strongly influenced by polymer molecular weight [105,106] and polydispersity [107,108]. Atomic force microscopy was used to examine PBTTT-C12 (low molecular weight Mn=10 kDa), which had a rod-like microstructure. A polymer chain's length and breadth are proportional to the number of π-stacked polymer chains that make up each rod-like domain, which is considered to be made up of rod-like polymer chains. After annealing at 100°C, the biggest molecular weight polymer (18kDa) was found to be polycrystalline with molecular terraces. When the polymer molecular weight rises, DSC tests show that a well-defined high-temperature mesophase to isotropic transition occurs at about 210°C with a melt temperature of 170°C. In contrast, a low MW polymer film consists of separate rod-like domains, whereas a high MW polymer film has a lengthy chain. Due to their interconnected nature, high-MW films have a high charge carrier mobility [109]. Thienothiophene polymers featuring interdigitated side chains have a thermotropic liquid crystalline phase as a result of side-chain melting. Up until the main chain melting temperature rises above the side chain melting temperature, mesophase is present. According to the research, PBTTT-C14 has a mesophase temperature range of 120-180 °C, which indicates smectic-like order [110].

1.4.1.6 Conducting-Polymer composites

Conductive-Polymer composites (CPCs)include conductive fillers in a polymer [111,112]. CPCs are used in conduction, sensing, EMI shielding, and as an inhibitor to triboelectric charging due to their easy manufacturing, low cost, and adaptable electrical properties[113-116]. Because most host polymers are insulating, CPCs rely on uninterrupted conductive networks generated after adding conductive fillers [117,118]. When the amount of conductive filler in the CPC material reaches a certain level, an insulator-to-conductor transition will occur; as early conducting channels emerge, and thus conductance increases. The percolation threshold φ_c determines this essential volume fraction. The polymer matrix develops additional electrical pathways as the conductive filler levels increased, allowing the conductance to increase until saturation. The following equation describes the electrical conductivity of CPC materials[118,119]:

$$\sigma = \sigma_0(\varphi - \varphi_c)^t \qquad (1.1)$$

where t is the CPC dimensionality exponent, σ indicates the electrical conductivity of CPC, and φ is the volume concentration of the filler. The parameters t = 2 and t = 1.3 in this model, respectively, for three-dimensional (3D) and two-dimensional (2D) CPCs.Experimental values sometimes diverge from predicted values. Among the traditional CPC fabrication techniques, melt mixing technologies, are the most frequently used to make commercial CPC materials [120,121]. Theoretically, the percolation value φ_c of 10–20 vol per cent corresponds to the spherical, randomly dispersed fillers [122,123]. Large-aspect-ratio semiconducting nanomaterials, such as graphene nanosheets or carbon nanotubes, offer a high surface area that can support good transportation systems, but their strong agglomeration propensity during treatment in host polymers results in a high φ_c. High φ_c CPCs have high melt viscosities, limited economic affordability, and poor mechanical characteristics (particularly ductility and toughness) [124,125]. Therefore, it has long been a major issue to efficiently reduce φ_c during the production of highly efficient CPC materials. Polyaniline, polypyrrole, polythiophene, poly (vinyl alcohol) (PVA), poly(vinyl chloride), and other conducting and nonconducting polymers have been used to make conducting composites and nanocomposites.

1.4.1.7 Graphene polymer composite

As a result of their high mechanical strength and stiffness, as well as their outstanding thermal and electrical conductivity, carbon-based nanofillers have been extensively used in the fabrication of nanocomposites with polymer matrices. Carbon black (CB), carbon nanofibril (CNF), carbon nanotube (CNT), and graphene are only a few examples [126]. One atom thick, graphene is a two-dimensional carbon layer with sp^2 bonds [127]. A honeycomb structure made up of individual carbon atoms is created [128]. It is possible to pass electrical current via the carbon atom's fourth outer-shell electron since only three are needed to form chemical bonds. The high electrical conductivity of graphene is attributable to the existence of electrons that may move at an incredibly fast rate. Graphene also has an extremely low aspect ratio due to its monolayer structure. There is new evidence to support the notion that fillers with very low or extraordinarily high aspect ratios have incredibly low percolation thresholds [129]. When graphene or carbon nanotubes are combined with a polymer matrix, conductive networks may be formed at very low filler concentrations. Percolation limits for graphene have been reported as low as 0.1 vol. per cent [130]. Graphene is often easier to make and less expensive to mass produce than carbon nanotubes. This offers graphene an advantage over carbon nanotubes in terms of uses. Recent studies have revealed low percolation thresholds and a substantial increase in effective electrical conductivity as graphene loading increases [131]. Researchers want to produce graphene-polymer nanocomposites for these reasons. Recent studies have demonstrated low percolation thresholds and a considerable increase in enhanced electrical mobility as graphene filler dosage increases. Exfoliating graphite to a single layer creates graphene [132,133]. Full graphite exfoliation and homogeneous graphene dispersion are challenging to achieve. Graphene agglomerates are created by layering and clustering graphene. Epitaxial chemical vapour deposition (ECVD) is another approach [134]. Different process factors, such as graphite oxidation and sonication energy, as well as interaction energies between graphene, matrix, and (if present) surfactant, might impact graphene clustering. By chemical means, graphene can be synthesized in bulk form. The most common approach is graphite exfoliation via graphite oxidation which leads to graphite oxide in which graphene oxide layers are held together through van der walls forces [135-137]. Graphene oxide shows a similar carbon structure to graphene but also has various oxygen functional groups [138]. The hydrophilicity of GO makes it a

suitable material to form a uniform thin film in electronics applications [139,140]. By using an appropriate reduction process, GO may be transformed into reduced graphene oxide with fewer oxygen functional groups [141]. Although some defects are still present in the restoration of graphitic structure [142]. In this thesis, we synthesized GO by an improved hummers method having fewer defects in graphitic planes[143]. The properties of thin films of GO and rGO can be modified by varying the coverage of sheets, chemical composition, thickness of the film, size of flake, and morphology of the film. GO and rGO nanosheets show nearly identical properties and can be tuned into conducting, semiconducting, and insulating thin films by adjusting deposition and reduction parameters [144,145].

1.4.2 Electrochemical sensing devices

A sensor is a device that detects alterations in its environment as a result of analyte interaction and converts these changes into a readable signal. Sensors are classified into two types based on their components: transducer and receptor. The function of the receptor is to interact with target(analyte) molecules among the various analytes present and thus make the sensor selective. The function of a transducer is to convert one form of energy into another. The changes which occurred between the analyte and receptors are converted into a readable signal like the voltage, current, resistance, light, etc.

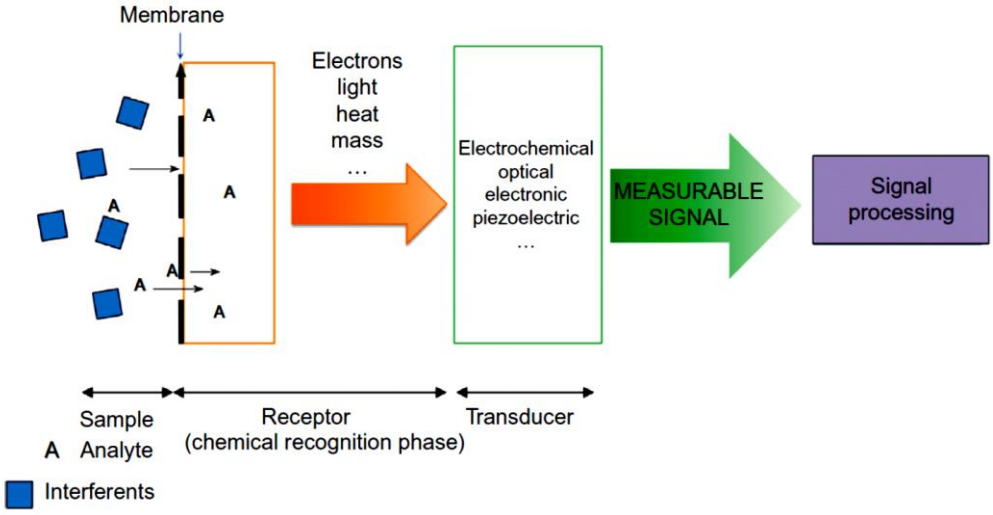

Fig.1.12 Schematic depiction of the working principle of a chemical (biochemical) sensor [146].

Reference, counter, and working electrodes make up an electrochemical sensor. It quantifies analyte-electrode reactions. Conductometric means a change in conductance, voltammetric means a change in current with supply voltage, amperometric means a change in current with time at a constant applied potential, potentiometric means a change in membrane potential, and impedimetric means a change in impedance relying on electrical amplitude for recognition. Because analyte-electrode surface contacts are sensitive to surface type and topology, the design of an electrochemical sensor must maximise analyte-electrode surface interaction while minimising interference-electrode surface interactions.

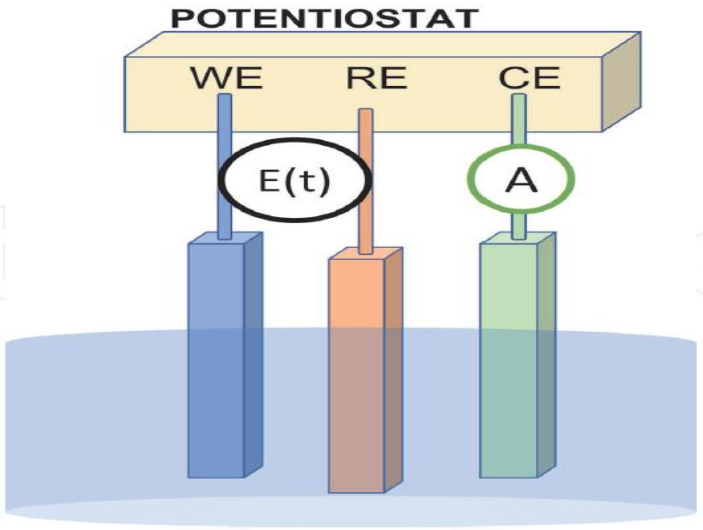

Fig.1.13 A working electrode (WE), a counter electrode (CE), and a reference electrode comprise an electrochemical system (RE). The working and reference electrodes are connected with a voltage E(t), and the current at site (A) is measured [147].

1.4.2.1 Parameters of Sensors

Several criteria are used to describe sensor quality:

(i) **Sensitivity**- It's the change in measurement signal per unit of analyte concentration.

(ii) **Detection limit**- The tiniest amount of analyte a sensor is capable of detecting at a particular signal-to-noise ratio. Without an analyte, the detection limit is three times the blank's standard deviation.

(iii) **Selectivity**- It describes whether a sensor reacts to a single analyte or to a collective of analytes that are present in a mixture. It is essential to a sensor's performance that it only communicates with the analytes being measured and not with any interference.

(iv) **Linearity**- It is defined as the deviation of a calibration graph produced empirically from a straight line. Ideal sensors have a wide concentration range and are linear.

(v) **Linear range**- The span of analyte concentrations for which the response of the biosensor varies linearly with increasing or decreasing concentration.

(vi)**Response time**- It's the amount of time it takes for a sensor to respond from zero concentration to a significant change in input value(analyte concentration). For real-time sample analysis, the reaction time of an ideal sensor should be as short as possible.

(vii) **Resolution**- When the composition is changed continually, the lowest concentration difference can be resolved.

(ix)**Stability**- It refers to the amount of time that a sensor retains its performance.

(x) **Life cycle**- The amount of time that the sensor will be active. It's important to distinguish between maximum storage (shelf life) and maximum operating life.

1.4.2.2 Advantages of electrochemical sensors

Several advantages of electrochemical sensors are as follows-

1- They give powerful analytical techniques with the advantages of quick, accurate, and unique analyte diagnosis.

2- They translate information about reaction characteristics between analytes and sensors into analytically usable signals.

3- They detect a broader variety of analytes and are low-cost, robust, and highly repeatable.

4- They're adaptable and can be built into compact portable devices with specially designed materials for real-time sample analysis.

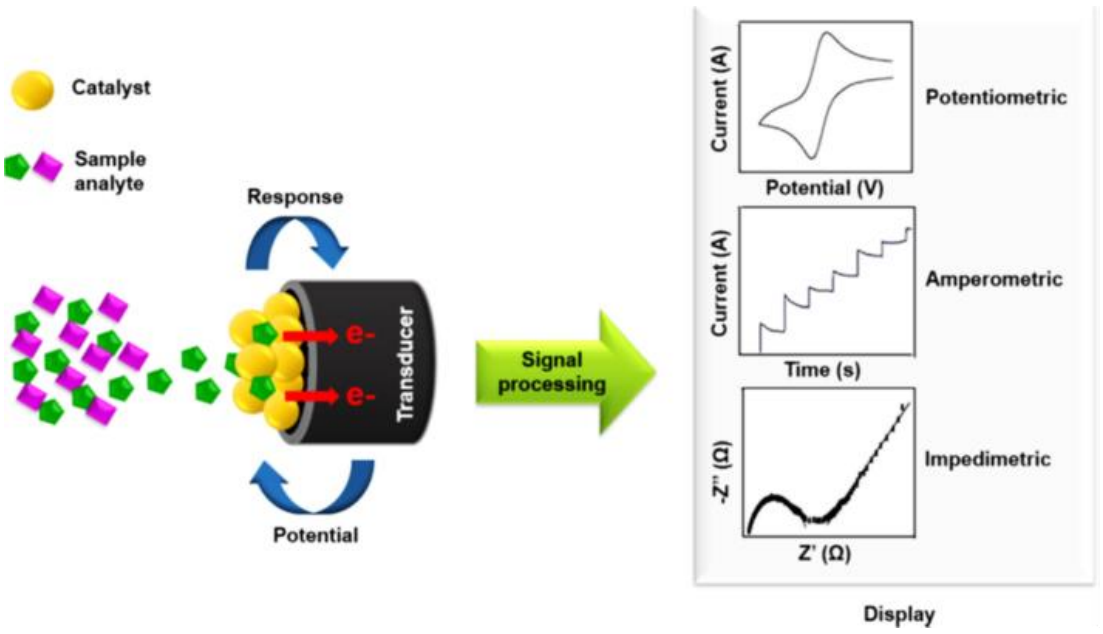

Fig. 1.14 Operating principle of an electrochemical sensor [148].

1.4.2.3 Review of the literature on electrochemical sensors based on carbon compounds produced from biomass

Carbon's chemical stability, large specific surface area, cytocompatibility, high electrical conductivity, and great mechanical strength make it a popular electrode material. Carbon black, graphite, carbon nano allotropes, and other kinds of carbon material are commonly employed in sensor applications [149]. By generating flaws and attaching various functional groups to the surface, the sensitivity with lower detection limits and selectivity may be improved. Nanomaterials have a huge surface area, which increases sensitivity when their atoms are exposed to the environment. Their excellent mechanical qualities make them perfect for use in electrical equipment. Low-dimensional crystals, such as graphene and carbon nanotubes, have surface characteristics that are simpler to regulate and amend than polycrystalline structures, resulting in high carrier mobility [150]. Synthesizing such materials as carbon nanotubes, fullerenes, and carbon nanofibers requires cumbersome steps. Chemical vapour deposition [151], wet spinning [152], and dry drawing [153] have all been utilised to create aligned carbon nanotube arrangements. These approaches are successful, but they are not cost-effective when used on a big scale. Chemical and mechanical peeling, epitaxial growing i.e. forming a crystal layer of one material on the crystal base of another material with the same crystalline orientation as the substrate, and chemical vapour deposition are all steps in the synthesis of graphene, which has a large surface area [154-157]. Because it is poorly soluble in water, it demands further functionalization such as hydrophilic carboxylic groups, alkyl amines, and amphiphilic polymers [158]. As a result, researchers are currently concentrating their efforts on developing lucrative methods for manufacturing carbon compounds from renewable sources. Because of its facile processability, cost-effective synthesis, richness in nature, lower toxicity, chemical inertness, and customizable pore size/surface characteristics, biomass has gotten a lot of attention [159-162]. Biomass refers to resources obtained from plants, animals, and marine organisms [163,164]. Water treatment [165,166], CO_2 capture [167,168], catalysis and energy storage [169,170], sensing [171,172], hydrogen storage [173,174], and other applications have all used biomass and biomass-derived materials. Often referred to as lignocellulose biomass, plant-based biomass is made up of cellulose/hemicellulose and lignin/tannin [175].

1.4.2.5 Selection of Bio-mass precursor (raw material)

The performance of activated carbon depends on starting materials used for its production in addition to the above-mentioned activation methods. Different sources can be used to derive activated carbon like plants, animals and minerals. The choice of selecting precursors mainly depends upon availability, price, purity and also on the manufacturing process proposed for the application of the product. Currently, agricultural wastes as biomass precursors have been utilised to synthesize activated carbon because of the low cost, highly abundant, renewable source and environment friendly. Activated carbon sold on the market is often made from resources such as wood, coal, peat, lignite, and waste petroleum products; these are all resources that are both expensive and restricted. This paved the way for the production of activated carbon from waste products from agricultural production (lignocellulose materials). It is possible to extract activated carbon from any part of the plant, including the root, the leaf, the bark, the flower, the fruit peel, the husk, the stem shell, etc. Woody materials and non-woody materials make up the two categories that are used to classify these waste products. Lignocellulose, lipids, protein, sugar, water, hydrocarbon, starch, and functional groups that can remove pollutants are examples of non-woody resources. Cellulose, hemicellulose, and lignin are the primary components of woody resources. According to Amirza et al., when it comes to the production of stimulated carbon, researchers are more likely to employ nonwoody farm rubbish than they are to use woody farm wastes [176]. The choice of a raw precursor is determined by satisfying seven fundamental criteria [177].:

(i) A high carbon content.

(ii) Low ash is caused by a lower proportion of inorganic materials.

(iii) Volatile matter content and high density.

(iv) A plentiful supply of raw materials is constantly available at a reasonable cost.

(v) Potential activation ability

(vi) Stability in storage

(vii) Producing a high-yield activated carbon

Biomass wastes, on the other hand, have a lower carbon concentration than fossil fuels. Regardless, the cheap cost of raw materials has a significant influence on % the output in industrial applications.

1.4.2.6 Pore size categorization

Micropores, mesopores, and macropores are commonly found in activated carbon's structure. These pores are crucial in determining how well-activated carbon performs in diverse applications. The International Union of Pure and Applied Chemistry has identified three different categories of activated carbon pore diameters: micropores(<2nm), mesopores(2-50 nm), and macropores(>50nm). Pores are also classified based on how accessible they are to the outside world. Open pores are those that interact with the outside world. Molecules or ions in the environment have access to them. Some pores may only be open on one side. Blind (dead-end, or saccafe) pores are the name given to them. When porous materials are heated for an extended period, sections near the outside shell of the pores disintegrate, resulting in closed pores with no connections to the outside world. Inadequate gaseous material discharge may also result in closed pores. The closed pore affects solid mechanical characteristics but not molecular physisorption or permeability. Geometry classifies pores. Kaneko classifies pores by their geometrical shapes: cylindrical, slit, cone, and ink-bottle [178].

1.4.2.7 Physicochemical property of activated carbons

The porous architecture of activated carbon contains a tiny fraction of various heteroatoms. The porous structure is activated carbon's most distinguishing physical characteristic. The chemical property is defined by the existence of surface functional groups with distinct atoms at the borders of basal planes.

(a) Porous structure's relevance

The carbon frame is made up of a combination of graphitic crystallites and an amorphous phase that includes complex aromatic and aliphatic forms. A few parallel plane layers of graphite formed the crystallites. The sp^2 carbon-carbon bond structure of the graphite surface is disturbed by activation, resulting in free valencies. Activated carbon has a structure that looks like a stack of aromatic sheets (crystallites) that are irregularly aligned and separated by unorganized carbonaceous materials. The existence of voids is connected to anisotropic crystallite alignment. When crystallites are activated, the spaces between them become free of less systematised carbonaceous phase with some carbon from the crystallites, forming channels, interstices, and fissures across the graphitic areas, resulting in a porous structure with diverse size ranges-micro,

meso, and macro. In various adsorption processes, molecules are held on the carbon top layer via physical encounters and/or chemical bonding. As a result, a high specific surface area is an important parameter in adsorption. The exterior of the activated carbons was made up of basal planes and the margins of planes that form the contours of microcrystallites. The presence of micropores accounts for the relatively large surface area values, and the majority of adsorption occurs in these pores. Although meso- and macropores are also important in the adsorption process because they provide a pathway for species to reach micropores, they play a minor role in the adsorption. Multi-layered physisorption from the vapour phase into a porous media continues until pore spaces in mesopores are filled with condensed fluid from the vapour phase, resulting in capillary condensation. Furthermore, the specific surface area is affected by the size of the molecules. Large molecules can induce molecular sieve effects because the pore circumference is less than the adsorbate molecules or the design of the pores prevents the adsorbate molecules from penetrating further into the micropores, such as tiny hole micropores generated are not approachable by spherical molecules. This demonstrates that a carbon's specific surface area is not inversely related to the activated carbon's adsorption capability. As a result, the distribution of pore sizes is a crucial factor to consider. In general, extremely microporous carbons are prioritised for gas and vapour adsorption, as well as the demarcation of gas molecules of various sizes provided the carbon has a proper allocation of small holes (molecular sieves), whereas fully developed meso- and macroporosity is ideal for solute adsorption from solutions.

(b) Surface chemistry's Importance

A large exterior area and a vast pore size allocation are said to be required for adsorption on the carbon surface. Even though carbons with similar morphological properties have different adsorption capacities with the same adsorbate [179]. Because of these variations, enhancing the adsorption capacity of activated carbons requires a proper porous crispness, which is a needed but not enough condition. It's also necessary to count the number and identity of surface functional groups. The presence of unpaired electrons at the periphery of basal planes indicates that the carbon atoms are unsaturated. When such sites are bonded to heteroatoms, various surface groups form. Oxygen-containing functional groups predominate at the carbon surface. In general, activated carbons have a large contour area, which results in a high chemisorption

affinity. As a result, when oxygen molecules interacted with carbon atoms, oxygen functional groups formed. Other oxidising agents, like O_3, CO_2, HNO_3, H_2O_2, and others, produce oxygen functional groups in the same way as molecular oxygen does. Surfaces of activated carbons can therefore be altered using heat treatment or various reagents [180]. Hydrogen, like oxygen, is located near the edges of carbon atoms on the surface. Additionally, N-functionalities can be added to activated carbons by the use of ammonia, melamine, or urea, all of which have unique properties. Depending on the oxidation circumstances, the type and quantity of distinct surface oxygen-containing carbon groups can change. Changes in the chemical composition of activated carbon can modulate its adsorption capacity. In the interaction of carbons with various adsorbates, surface groups play an essential role. Two key impacts should be noted. One is the adjustment of the carbon's hydrophobicity/hydrophilicity. Carbon atoms are often hydrophobic. The inclusion of polar oxygen functional groups that can form hydrogen bonds with water molecules, improves hydrophilicity. This effect is critical for the solution to permeate the carbon surface. Because moisture (water molecules) interacts with oxygen functions, the adsorption of the gas into the micropores may be hampered, reducing the adsorption performance of activated carbon. The impact of surface functional groups on the acidity or basicity of carbons is another crucial aspect to take into account. ACs have both acidic and basic spots on their surface, making them amphoteric. When the pH of the medium exceeds the pKa of these groups, i.e. when the medium is basic, most oxygen functional groups act as acidic groups. However, the primary basic sites on the carbon surface are pyrone-like and chromene-like groups [181], as well as the delocalized π-electrons of the basal planes [182]. Several nitrogen-containing features and functionality can also act as basic sites. As a result, if the acidic groups outnumber the basic groups or have a higher overall acidic power, the carbon will be acidic, and vice versa. Another critical factor is the medium's pH in relation to the activated carbon's point of zero charge (pH_{pzc}). When the pH rises above pH_{pzc}, acidic functionalities degrade and release protons into the media, culminating in a net negative charge on the carbon. When the pH is less than pH_{pzc}, basic sites merge with protons from the medium to form a positively charged surface. As a result, changing the chemistry of the carbon surface can increase interactions and adsorption capacity. As a consequence, basic carbons will preferentially adsorb acidic molecules, whereas acidic carbons will preferentially adsorb basic chemicals. Furthermore, cations will be

accepted if the carbon layer surface is negatively charged, whereas anions will be accepted if the carbon layer surface is positively charged.

1.4.2.8 Biomass-derived carbon (BDC)-based electrochemical sensors: a survey of the literature

The two most common experimental methodologies for BDC as electrochemical sensors are voltammetric and amperometric. BDC-based electrochemical sensors are categorised in the following area according to the type of analytes.

(a) Species of organic origin

Using BDC-modified electrodes, biologically active compounds (such as ascorbic acids, glucose, and amino acids) and contaminants of organic origin (such as pesticides, nitrophenols, and bisphenol A) were determined.

(i) Amino acids

By pyrolyzing the kenaf stem at 900 °C, Wang et al. created a macroporous carbon-based sensor for the electrochemical diagnosis of cysteine and N-acetyl cysteine [183]. Co NPs are widely dispersed due to the honeycomb structure's vast surface area (1019 m^2g^{-1}), which improves electroanalytical efficiency through in-situ conversion of Co NPs into CoO_2, which acts as a catalytic site in 0.1 M NaOH. Cysteine and N-acetyl cysteine had broad linear ranges of 0.10–18.60 mM (LOD 0.05 mM) and 0.15–26.24 mM (LOD 0.02 mM), respectively.

Han et al. used H_3PO_4 to make nanoporous carbon from Dandelion pappus by pyrolysis at 700°C after chemical stimulation with H_3PO_4 (in an N_2 atmosphere). For the examination of Tryptophan, nanoporous carbon is utilised as an electrode material [184]. The porous framework and huge specific exterior surface area of nanoporous carbon resulted in superior electrocatalysts for Trp oxidation, with a fairly low overpotential and improved current responsiveness. The amperometric response of the NPC-based sensor has linearity in the concentration range of 1 μM to 103 μM, with a sensitivity of 171.43 μA mM^{-1} cm^{-2}. The suggested sensor has also been used to determine Trp in actual samples, with good results.

(ii)Glucose

Rapid and sensitive glucose measurement has been an important challenge in healthcare monitoring in recent decades. As a result, efforts have been made to develop and commercialise non-invasive glucose biosensors [185]. The selective oxidation of glucose in the presence of glucose oxidase (GOx) [186,187], followed by the determination of amperometry [188], is how enzymatic sensors work.

Metal/metal oxide NPs are used in non-enzymatic sensors to catalyse glucose oxidation with good selectivity and sensitivity [189,190]. Because of their stability under a variety of pH, humidity, and oxygen conditions, non-enzymatic sensors outperform enzymatic sensors. Even when GOx-supported BDC-modified electrodes are used for glucose sensing, such factors have a significant impact on enzymatic activity. As a result, enzyme-based electrodes are only mentioned in a few instances.

Chen et al. introduced a glucose sensor using MWCNTs coated on carbonised silk textiles decorated with Pt microspheres and GOx. Sensor sensitivity is 288.86 μA mM^{-1} cm^{-2} and the linear range is 0 to 5 mM, according to the results [191].

Bendable BDC-modified electrochemical sensors were used to analyse six biomarkers identified in sweat [192]. For efficient electron transport and good access to reactants, the N-doped graphitic structure and hierarchical porous carbon structure generated from silk fabric had strong electrical conductivity, plentiful active sites, and good water wettability. Because of these characteristics, the suggested electrochemical sensor was chosen as the working electrode. The flexible, multimodal sensing patch was also paired with a signal collecting and transmission circuit component to create a wireless, on-body, real-time sweat analysis patch. Despite the above advancements, better sensor performances are obtained using non-enzymatic platforms. Despite the aforesaid developments, non-enzymatic systems provide greater sensor performance. Through activating several electrocatalytic pathways, cobalt and nickel-based catalysts such as Ni [189,193], CuNi [189], and Co_3O_4 [190] were employed to increase sensing capabilities. Ni is the most studied substance because the in-situ production of Ni oxides and oxyhydroxides allows for the selective catalytic performance oxidation of glucose into gluconolactone [193]. Wang et al. constructed a 3-D porous carbon/Ni nanoparticles nanocomposite [189] and a CuNi NPs-containing BDC-based carbon paste electrode [183]. The suggested approach is a green analytical process because of the low pyrolysis temperature and minimum usage of reagents. Veeramani et al. have

created a doped activated carbon and then form nanocomposites with nickel oxide for glucose detection that do not need enzymes [193]. The increased activity of this modified sensor is due to the synergistic action of NiO nanoparticles and HAC loaded with heteroatoms. Madhu et al. described the porous carbon-cobalt oxide composite as an enzyme-free modified electrode for glucose monitoring [190]. The biomass precursor for the creation of activated carbon is the pongam seed shell. Outstanding sensitivity and detection limits of 34.2 $\mu A \mu M^{-1}$ cm^{-2} and 21 nM have been suggested for the glucose sensor. The electroanalytical performance is due to Co_3O_4's catalytic performance on porous activated carbon, which allows for fast electron transport suited for industrial applications.

(iii) Ascorbic acid, dopamine and uric acid

Ascorbic acid (AA), dopamine (DA), and uric acid (UA) were also found in body fluids[194,195]. The BDC surface's large specific surface area and enrichment with N-containing functional groups may operate as active oxidation centres [196,197]. No enzymes or metals are required to increase sensor selectivity [198,199]. Vediyyapan Veeramani et al. made activated carbon from pumpkin stems for biomolecule detection [199]. AC was generated by carbonising pre-treated fried pumpkin stems with 10% $ZnCl_2$ for 2 hours in N_2. AC-700's BET surface area was 793 m^2g^{-1}. The AC-700 modified electrode outperformed the other AC-modified electrodes and RGO during biomolecule detection. The higher catalytic activity of biomolecules in biomass-derived AC is due to their larger surface size, tiered pore size distribution, and predominance of chemical groups such as heteroatoms (83.427 per cent C, 1.085 per cent N, 0.383 per cent S, and 0.861 per cent H). Zhang et al. created a microporous carbon electrochemical sensor ($ZnCl_2$-CF/GCE) using Kiwi skin to detect biomolecules (AA, DA, UA) [198]. To make $ZnCl_2$-CF, kiwi peel and $ZnCl_2$ were carbonised at 800 °C. BET surface area is 1226 m^2g^{-1}. $ZnCl_2$-CF showed remarkable sensitivity and selective signalling with linear response ranges of 0.05–200 µM, 2–2000 µM, and 1–2500 µM, respectively. LOD (S/N=3) were 0.02 µM, 0.16 µM, and 0.11 µM.

In comparison to bare GCE, the morphological characteristic and high surface area assist the AA peak towards greater negative potentials with increased current. These results are comparable to non-biomass materials [200,201]. Similarly, AA was measured amperometrically in various matrices [202-204]. Li et al. used pyrolyzed

pulverised cherry husks to alter GCE [203]. The material's electrocatalytic capability was shown by reducing the oxidation overpotential from 0.399 V on bare GCE to 0.026 V on the recommended electrode. Using this principle, electrodes based on carbon nanosheets (made by carbonising okara wastes [202]) and carbon nanorods (obtained from pyrolyzed apples [204]) exhibited significant performance, similar to nanomaterial-based electrochemical biosensors [205,206]. Using pliable electrodes built on carbonised silk fabric, selective and sensitive dopamine detection was recently reported [207].

(iv) Phenolic compounds

Phenolic compounds are utilised in industrial applications (for example, the synthesis of plastics, insecticides, and pharmaceuticals), and their release into the environment pollutes the ecosystem. Human health is jeopardised even at tiny levels of these chemicals. As a result, a variety of approaches[208] have been used, including electroanalytical techniques using biochar-based electrodes to identify phenolic chemicals. Bisphenol, in this context, is a severe hazard to the environment and human health, and it has been determined using a variety of ways. BPA detection has been reported using both non-enzymatic [209] and enzymatic sensors [208,210]. Enzymatic sensors produced the best results in terms of sensitivity.

Yujuan Xu et al.[209] created a bamboo fungus-derived NDC for enzymless electrochemical detection of Bisphenol A. (BPA). NDC's high N-atom content, porous structure, and high conductivity helped oxidise BPA. BPA oxidation may be promoted by doped nitrogen active sites, whereas BPA adsorption and accumulation were boosted by the porous structure. Differential pulse voltammetry quantified BPA (DPV). Within 1.0 M to 50.0 µM, LOD was 1.068 µM (S/N = 3).

The NDC/GCE method was also successfully used to determine BPA levels in soil extract samples. Biochar-modified enzymatic biosensors have also been created recently. These systems utilise Tyrosinase (Tyr) as a selective enzyme for BPA oxidation [212]. Liu et al. created an enzyme-based detector based on BDC particles (BCNP) produced from sugarcane for the detection of bisphenol A (BPA) [211]. Due to their large surface areas, enhanced conductance, and biocompatibility, BCNPs/Tyr/Nafion/GCE performed electroanalytical better and has a linear range of the suggested sensor is 0.02 to 10 µM and LOD of 3.18 nM.

He et al. reported the immobilisation of an enzyme (Tyrosinase) on magnetically functionalized BDC particles (ML-TYR/Mag-BCNPs-COOH) [210]. Slow pyrolysis in an inert environment produced BDC particles from Bagasse biomass. The Mag-BCNPs-COOH composite was then formed following functionalization and subsequent magnetisation with Fe_3O_4. The magnetic characteristics of the multi-layered Tyr film favoured stable immobilisation. In comparison to the single-layer system, the multi-layered system's high-concentration enzyme resulted in good biocatalytic activity. The lowest detection limit for BPA detection is 2.78 nM, with an acceptable linear range, which may be attributed to the biosensor's exceptional features and comparable to the enzymatic electrodes founded on reduced graphene oxide [212] and carbon nanotubes [213].

Madhu et al. made activated biochar from mango leaves (Mangifera indica) to detect 4-nitrophenol (4-NP), an environmental contaminant [171]. Improved catalytic activities and reversible redox behaviour during 4-NP detection are provided by the large surface area (1555 m2g-1) of biomass-derived AC with rich functional groups. Over AC-modified GCE, a linear connection was detected between cathodic peak current and 4-NP concentration up to 500 µM, with 0.16 µM LOD and 5.810 µA μM^{-1} cm^{-2}sensitivity.

Rabina Bhujel et al. have created a biomass-derived silver ornamented graphene (AgGr) using onion peels recovered from fresh onion (Allium cepa) [214]. The biomass-derived silver decorated graphene (AgGr) samples are manufactured in an APCVD reactor at temperatures ranging from 600 to 800 °C. Due to its many active sites and flaws, AgGr-800 is the least helpful for p-nitrophenol sensing.

Over bare [215] and gold nanoparticles spread on BDC-modified GCE [216,217], the poisonous dihydroxybenzene isomers hydroquinone(HQ) and catechol(CT) were also examined. Ferreira et al. determined comparable chemical molecules using a BDC(BC) based electrode made from Babassu petiole pyrolysis [215]. The square wave voltammetry of the combination HQ and CC revealed over-lapped peaks over GCE, although the sensor BC600/GCE modified electrode provided a resolution of Ep=0.14 V. HQ and CC peak currents on BC/GCE were also three and five times greater than on plain GCE. When the BC600/GCE electrode was employed, the HQ and CC electrodes shifted towards a more positive potential. Because of the presence of active sites (hetero atoms carrying functional groups), BC demonstrated higher peak-to-peak separation, sensitivity, and electrocatalytic activity, increased electroactive surface area (specific

surface area = 300–400 m^2g^{-1}) The adsorption-controlled electrochemical process can be used to explain such phenomena [218].

It also created Au NPs embellished BDC-based sensors for HQ and CT sensing. Jinshou Wang et al.stated gold nanoparticles decorated BDC (WBC/Au) synthesised from white myoga ginger biomass [216]. The 850°C nanocomposites measured HQ and CC concurrently with low detection limits and great sensitivity. High quantities of C-O/N-O, C=O, and COOH/COOR bonds and Au NPs may explain WBC/Au-850 effectiveness.

Gold NPs decorated into porous BDC (Au-NPs/BC) were reported by Yunhui Xiang et al. from Dracaena sanderiana biomass [217]. The Au-NPs/BC) nanocomposites were generated with excellent porosity, high specific surface areas, and strong electrical conductance, allowing for simultaneous assessment of hydroquinone and catechol with low detection limits (in the nanomolar range) and high sensitivities. Kalinke et al. created an electronic tongue for catechol (CAT), 4-ethylcatechol (4-EC), and 4-ethylguaiacol (4-EG) phenolic chemical discrimination and stripping voltammetric detection [219]. The suggested sensor array has analytical potentiality, allowing chemometric processing to distinguish and determine CAT, 4-EC, and 4-EG. For the three chemicals tested, the technique demonstrated sensitivity, repeatability, and high linearity (R^2>0.9940). All three sensors allowed for the spontaneous preconcentration of three compounds, indicating that they might be used as passive samplers for phenolic component assessments in wine and food samples. Veeramani et al. employed food chemistry to detect catechin [220] and vanillin [221]. Veeramani et al. created sheet-like porous activated carbon (GPAC) from Bougainvillea flower using $ZnCl_2$. High-sensitivity GPAC catechin detection (CA) is found. The suggested sensor offers excellent sensitivity, a broad linear range, and a low LOD for CA detection. GPAC's real-time CA detection was tested using green tea leaves. Veeramani et al. made Cajeput tree bark-based activated carbon(TBAC)from Cajeput tree bark to quantify vanillin [221]. TBAC's electrocatalytic activity for vanillin oxidation is due to its wide surface area and porosity. The vanillin sensor has a broad linear range (5–1150 µM), low LOD (0.68 µM), and high sensitivity (0.32 2µA μM^{-1} cm^{-2}). Compared to earlier investigations, the findings aren't impressive [222,223]. Human urine phenolic medication detection has gained interest.

Kim et al. described an electrochemical sensor constructed from biomass-derived carbon material for detecting Acetaminophen, also known as paracetamol, an antipyretic and analgesic medication [224]. Because acetaminophen (AC) can produce dangerous metabolic changes in the human body, it is critical to detect even small amounts in the body. Two-stage activation procedures were used to prepare the electrode material. After being dried, the kelp powder was heated to 700°C (10°C/min) in an inert atmosphere for three hours. The ZAKC product was made by heating the KC from the Kelp carbon extraction to 700°C (10°C/min) under Ar flow for three hours and mixing it with $ZnCl_2$. The ZKAKC product was created by heating KOH and pre-activated carbon in an Ar flow at 800 °C (10 °C/min) for one hour, resulting from the second activation. Electrode materials are made of ZKAC. Increases in pore capacity and specific surface area were achieved by the activation process. When it came to the detection of acetaminophen, the modified electrode proved to have excellent sensitivity, selectivity, and an excellent LOD of 0.04 µM. Even in the presence of ascorbic acid and dopamine, the redesigned electrode could detect acetaminophen at a limit of 0.007 µM. Nevertheless, due to the extensive preparation procedure, this was a more time-consuming project than others that had previously been published

Cheng et al. carbonised oyster mushrooms to generate Au-Pt@BPC [225]. Baicalein's electrochemical response (LOD = 10 nM) was improved by the Au-Pt@BPC-altered carbon ionic liquid electrode (CILE). This is because of the Au-wide Pt@BPC's surface area, multilayered porous structure, strong metal conductance, and catalytic performance. The outcome falls short of that of earlier studies [226].

(b) Inorganic chemical electrochemical sensors

(i) Trace metals

The toxicity of metals and their widespread dispersion into the surroundings affected the design and fabrication of electrode materials for their detection [227]. The majority of studies revealed concomitant detection of the dangerous metal ions Hg^{2+}, Cu^{2+}, Cd^{2+}, Pb^{2+}, and Ni^{2+} in analytes with a nanomolar limit of detection, which is comparable to extremely complex instruments (such as ICP-MS) and other electrodes not based on biomass [228]. Madhu et al. utilised dead mango leaves to generate carbon nanoparticles having spherical shape decorated activated carbon (SNAC) for detecting heavy metal ions [229]. Cd(II), Pb(II), Cu(II), and Hg(II) LODs at SNAC-modified

GCE are 24,4, 5,73, and 24.6x 10^{-9} M, respectively. Pd-decorated BDC performed badly for the same analytes. Pd NPs, on the other hand, aid in the enhancement of conduction pathways [230,231]. The precise and concurrent monitoring of such analytes in these circumstances depends on the BDC's porosity.

Based on a spherical shell type bismuth oxide enriched mesoporous carbon aerogel nanocomposite from 900 °C maize flour pyrolysis, Zeinu et al. developed a supersensitive electrochemical sensor [232]. The electrode material demonstrated the lowest known detection limits for Pb^{2+} and Cd^{2+} utilising activated carbon under ambient conditions. Due to analyte adsorption and micro- and mesopores on the novel material, lead and cadmium have linear detection ranges of 0.5 to 10 pM and 15 to 100 pM, respectively. Real-world water analysis was also studied using inductively coupled plasma optical emission spectroscopy, and the findings were similar (ICP-OES).

Due to metal ion interference, the bare carbon-paste electrode [233] and the kelp-based AC electrode [234] both provided unacceptable analytical results. Voltammetry may be used to find the ions of Pb [235-237], Cd [238], Cu [239], Ni [240], and Zn [241] in a solution. With a LOD of 0.7 nM and a linear range of 1.5 nM-800 nM, Li et al. used biomass waste based on pitch pine at high temperatures under oxygen-limited conditions for Pb(II) detection [236]. Baikeli et al. created charcoal by carbonising almond shells in nitrogen [237]. Following the synthesis of nitrogen-doped nanoporous carbon (N-NPC) by a hydrothermal process utilising urea as the nitrogen source, nanoporous carbon (NPC) was created by activating charcoal with KOH. The most plausible reason for the enhanced electrochemical sensing capabilities is N-doping.

Bi-decorated electrodes produced good results with bare BDC electrodes for selective Pb^{2+} detection [235]. For the measurement of zinc(II) ions, Oliviera et al. modified a carbon paste electrode with a BDC produced from castor oil cake precursor and embellished with mercury ions [239]. Within a concentration range (LDR) of 5.0x10^{-7} to 3.0 x10^{-5} mol L^{-1}, zinc(II) ions showed a linear response, with detection and quantification limits (LOD) of 1.7x 10^{-7} and 5.8x 10^{-7} mol L^{-1}, respectively. Because Zn^{2+} reduction occurs at very low voltages, Hg electrodes are used in the process.

(ii) Hydrogen peroxides

Electrochemical sensors with excellent selectivity and sensitivity were developed as a result of the expanding interest in H_2O_2 evaluation in medical diagnostics, the food

industry, and other fields[204]. When it comes to electrochemical sensors, BDC-modified electrodes outperform those with a shorter lifespan [242].

Electroanalytical performance was improved by using BDC augmented with metal-based NPs to catalyse H_2O_2 redox reactions in two studies [243]. Li Wang et al. developed a 3-D macroporous carbon (3D-KSCs) derived from the kenaf stem for the detection of H_2O_2 [243]. Several 3D-KSCs/inorganic nanocomposites, including Prussian blue (PB) nanoparticles (NPs)-carboxylic group-functionalized 3D-KSCs (PBNPs-3D-FKSCs), CuNiNPs-3D-KSCs, and CoNPs-3D-KSCs, were created using either carbonization at one step of KS metal ion complex or a straightforward two-step method that consists of carbonization and additional chemical synthesis. The 3-D honeycomb structure, which has a substantial effective surface area, adequately enables a wide variety of electro-active entities, and greatly enhances mass and electron transport, leading to strong electrocatalytic activity toward matching target molecules. Advanced electrochemical sensors with great sensitivity, selectivity, and stability may be made using this arrangement. A CeO_2-decorated BDC that was generated from Jerusalem artichoke was developed by Bi et al. as a non-enzymatic platform for H_2O_2 sensing [404]. This platform has the lowest limit of detection (LOD) of all BDC-derived electrodes (30 nM).

Wax gourds (244) and apple-pyrolyzed carbon nanorods [204] are examples of non-decorated BDC-modified electrodes that have analogous topologies and specific areas (800–900 $m^2\ g^{-1}$) but lower efficiency. Enzymatically modified BDC electrodes were also used [245]. Horseradish peroxidase catalysed H_2O_2 reduction. This method is expensive, complex to prepare, and sensitive to pH and temperature.

(iii) Nitrites

Because high levels of NO_2 in the blood tend to oxidise haemoglobin, the nitrite ion is the most investigated analyte in the dietary and environmental fields [246]. Nanosized BDC worked best for nitrite sensing. Carbon nanospheres (CNSs) were made from Areca nut seeds using one-step pyrolysis at 550°C to detect nitrite [247]. The CNSs/GCE modified electrode displayed a current peak at 0.89 V with a downward shift in comparison to bare GCE in 0.1 M PBS (pH = 7.0) and 3 mM $NaNO_2$ solution. High catalytic activity may be due to CNSs' porous nature and improved adsorption sites. The linear behaviour of current with nitrite concentration from 0 to 5 mM

substantiated the CNSs/GCE electrode's good catalytic performance. Without extra activation or doping, CNSs performed better at nitrite oxidation, indicating that a good pyrolytic method might provide a material with improved characteristics quickly.

A comparable nanoscale morphology was investigated by Li et al. using nitrogen-enriched carbon dots (N-CDs) synthesised from kiwi seeds, white sesame seeds, and black sesame seeds [248]. N-CDs nanomaterials showed good electrocatalytic activity for nitrite detection, with a detection limit of 0.23 µM (S/N = 3). Similarly, Madhu et al. reported the same results utilising a HAC electrochemical sensor made from banana stems for the detection of nitrite ions [249]. Pre-treated banana stem powder was mixed with 10% KOH and heated in an N_2 environment at temperatures between 700°C and 900°C to produce activated carbon. Carbon, hydrogen, nitrogen, and sulphur concentrations in the synthesised HAC ranged from 61.12 to 2.567 to 0.4315 to 0.4349 per cent. The HAC material's well-developed hierarchical porosity nature allowed for rapid electron transfer, resulting in remarkable sensitivity and selectivity. HAC was an excellent choice for detecting nitrite at a very low level. HAC-modified GCE's nitrite sensor has a sensitivity of 9 or 13.2 µA $\mu M^{-1}cm^{-2}$, and its detection limit (LODs) is 0.07 µM. Due to the HAC's vast surface area and varied pore size, it acts as a reservoir for ion diffusion from the electrolyte, reducing ion diffusion lengths by up to 80%. Several water samples were successfully tested using the sensor's nitrite measurement capabilities. According to Cao et al. who also looked at Cu-decorated BDC for nitrite detection, their results were quite comparable [250].

1.5 Motivation and Objective of the Thesis

Carbon materials are a wide family of structures and textures that underpin a growing variety of applications, as seen by the vast number of articles published on the subject. Since 1900, there have been tens of thousands of publications. Strong covalent connections are formed when carbon-based materials are chemically mixed with other carbon-based materials and with a range of other elements, showcasing the flexibility of carbon-based materials. As a result, they have outstanding properties such as great strength, density, and hardness. Their investigation, creation, and development occur in a variety of fields, and research on the creation of carbon-based materials has produced several favourable discoveries for a variety of structures, enabling the manufacturing of several materials with varied uses. A new dimension is added to this field after the

introduction of 2-D carbon and carbon QDs nearly two decades back. These materials showed enormous potential in sensors and electronic devices. Nowadays 2-D materials are getting more attention in the scientific community due to their various advantages and ease of fabrication.

Taking these facts into account, as well as future uses of Carbon nanomaterials and their composites for device applications, the thesis' main goal is-

(i) To use diverse ways to synthesize low-cost 2-D carbon nanomaterials and polymer-carbon nanocomposites for device applications.

(ii) To utilise organic conducting polymer along with carbon as filler materials in the fabrication of cost-effective, ambient temperature functioning thin film transistors.

(iii) To ease the time-consuming thin film fabrication approach that has traditionally been utilised to make conducting polymer thin film transistors and their further use as a gas sensor.

(iv) To develop low-cost 2-D carbon materials produced from biomass having wide surface area, low toxicity, adjustable pores, excellent electrical conductance, chemical inertness, and the presence of functional heteroatoms for use in electrochemical sensing.

1.6 Organization of the thesis

The thesis is divided into **seven chapters**, one of which is the current chapter, which is titled "Introduction ". The following are the contents of the seven chapters of the thesis:

Chapter 1 gives a general idea and an introduction to some basic concepts about carbon materials, synthesis and their properties, the importance of polymer composite, charge transport in thiophene conducting polymer, the importance of techniques used in the fabrication of thin film of conducting polymer composite, development bio-mass derived activated carbon for electrochemical sensing application, the significance of nanomaterials-based sensors and the need to produce handheld, low-cost sensors for drugs used to treat crucial illnesses This chapter contains the results of an extensive literature review on these topics.

Chapter 2 covers the various experimental approaches used in the characterization of formed materials. Carl Zeiss Supra 40 SEM images were obtained for morphological

analysis (New Zealand).HR-TEM and SAED patterns, on the other hand, were obtained using a Tecnai G2 (New Zealand) over a Cu grid. FT-IR spectra were collected using a Thermo 5700 FT-IR spectrometer from Germany. The Raman spectrum was captured using an SPR 300 Raman spectrometer with a 532 nm exciting laser source. NT-MDT, Russia, was used to examine the AFM topographies, phase images, and KPFM of film in tapping mode. To obtain a structural study, powder XRD and GIXD of the thin film were performed using an advanced thin-film X-ray diffraction system grazing incidence in-plane diffraction (Rigaku, Japan) with focused Cu Kα radiation (λ= 1.54056Å). For each sample, the angle of incidence was set at 0.20°. Cyclic voltammetry (CV) and Differential cyclic voltammetry (DPV) setup have been employed for electrochemical characterization (Autolab, Metrohm, USA). Using a semiconductor device analyzer, the charge transport properties of fabricated OTFTs were investigated (Keysight B1500A). For pore size measurement and surface area, a BET surface area analyzer, Microtrac Beslorp, having30% N_2/He, N2; 0.15 Mpa; and power of 110/AC230 V, 400W, and 50/60 Hz was used.

Chapter 3 discusses fast-grown-up self-assembled polythiophene/graphene oxide nanocomposite thin coating at an air-liquid interface for good mobility polymer thin film. transistor. The vast surface area and nano-size thickness of GO confer significant improvements in the polymer's various properties. GO's exceptional framework and usable properties allow for charge transfer interactions with various organic conjugated polymer molecules. There is currently a lot of research going on in the advancement of organic polymer-based semiconducting materials like polyaniline, polythiophene or its derivatives, and so on. Among these, poly [2,5-bis(3-tetradecylthiophen-2-yl) thieno[3,2-b] thiophene] (PBTTT), a solution-processable derivative of polythiophene conducting polymer, has piqued research interests owing to its improved charge transfer characteristics and capacity to self-organize into an organized arrangement. Crystallization induced by π-π stacking, the interaction of alkyl side chains, and changes in solubility allow for an increase in crystallisation. As a result, to investigate the remarkable electronic properties of graphene nanosheets as well as the ease of processing and changeable electronic properties of PBTTT, we presented the use of a composite thin film of these two materials. Finally, electrical testing along the film in an OTFTs configuration reveals high mobility (0.112 cm^2/V.s), ∼10^3 on/off ratio, and other properties in ambient conditions. As a result, our research demonstrated a path to

rapidly growing self-assembled thin films of composite using the FTM technique for advancements in device performance and parameters such as high mobility.

Chapter 4 deals with the ordering and aggregation in poly [2,5-bis(3-tetradecylthiophen-2-yl) thieno[3,2-*b*] thiophene] [PBTTT] and is achieved by incorporating two-dimensional (2-D) reduced graphene oxide nanosheets into the polymer environment. At the air/liquid interface, thin films of PBTTT/rGO nanocomposites are formed by the rapid floating film transfer technique. Several characterization techniques corroborate the edge-on-oriented polymer nanocomposite thin film. Additionally, the polymer nanocomposite thin film is used to make organic field effect transistors (OFETs), which have better device efficiency in atmospheric conditions i.e. 0.26 $cm^2V^{-1}s^{-1}$ average mobility in saturation region at a drain voltage of -40 V and which is about 22 times that of pristine polymer(μ=0.012 cm^2 /V.s) and more than four times in on/off ratio ($\sim$1.3 $x10^3$). Our study reveals a way to rapidly generate high-quality nanocomposite thin films to improve gadget efficiency.

.

Chapter 5 deals with enhancement in the characteristics of polymer nanocomposites by using nanofillers that are based on carbon. These carbon nanostructures are of significance in nanocomposite research as well as other applications because of their extraordinary properties, which include a high Young's Modulus, tensile strength, electrical conductivity, and specific surface area. Such systems are portrayed as conductive networks created by a polymer matrix including conductive filler. Preparing composite materials with a low conductive filler loading, which retains the mechanical qualities of a polymer while providing high electrical conductivity, appears interesting. In the present study, Poly(2,5-bis(3-alkylthiophen-2-yl)thieno[3,2-*b*]thiophene)-Graphene quantum dots nanocomposite is formed by ultrasonication. A simple floating–film transfer method (FTM) is used to form a highly oriented thin film of polymer nanocomposite in organic thin-film transistor fabrication. At -40 V drain voltage, the average field effect mobility(μ) of PBTTT/GQDs nanocomposite OTFT is 0.16 cm^2/V.s, which is roughly 16 times that of pristine polymer (μ=0.0095 cm^2/V.s) and more than 2.8 times the on/off ratio of pristine polymer i.e. $\sim$0.56$x10^3$ under ambient conditions.

Chapter 6 deals with the Electrochemical Sensing of Roxarsone on Natural Biomass-Derived Two-Dimensional Carbon Material as a Potential Electrode Material. Organic arsenic, a less poisonous version of arsenic found in the advanced animal drug roxarsone (ROX) (3-nitro-4-hydroxyphenyl arsonic acid), is used to cure the parasite infestation coccidiosis and could be converted into inorganic arsenic. It is also transfused in chicken raised for meat intake in the poultry industry. Arsenic concentrations in the liver, muscle, and heart of chickens fed roxarsone-containing feed (20-40 mg kg^{-1}) were 37, 25, and 26 $\mu g kg^{-1}$, respectively. Many of the arsenic compounds released by animal waste are water-soluble, increasing the amount of inorganic arsenic in the surroundings and causing contamination. In different countries, tolerable arsenic levels in drinkable water range from 50 to 10 ppb. As a result, a thorough diagnosis of roxarsone has piqued the interest of researchers in food samples and human health-related platforms. Because of their low cost, good sensitivity and selectivity, rapid detection, and portability, electrochemical methods are extensively used in the tracking of multiple feedstuffs. Because of their high electrical conductivity, specific microstructure, and good stability, carbon-based materials have attracted a lot of attention as electrode materials. Because of their high surface area, low toxicity, adjustable pore size, good electrical conductivity, chemical stability, and the presence of heteroatoms that provide functionality, biomass-derived activated carbon materials have piqued the interest of experts. As a result, we postulated the formulation of meso/microporous activated carbon as a sustainable, eco-friendly, and simple-to-use material for electrode modification, and we intend to use it for electrochemical sensing of arsenic-based medicine ROX via DPV. The ROX sensor is configured and established to work well at 0.66 V (vs Ag/AgCl) under ideal conditions. The proposed sensor has a wide linear series (0.76-474 µM) with a detection limit in the nanomolar range (1.5 nM) and good sensitivity (0.0714 $\mu A \mu M^{-1} cm^{-2}$) on a glassy carbon electrode. 2D carbon-modified electrodes were successfully used in human blood serum samples to determine ROX (LOD = 1.8 nM).

Chapter 7 deals with the present work's summary/conclusions and the future scope of the work found in Chapter 7.